HHS Public Access

Author manuscript

J Magn Reson. Author manuscript; available in PMC 2022 April 01.

Published in final edited form as:

J Magn Reson. 2021 April ; 325: 106933. doi:10.1016/j.jmr.2021.106933.

Dynamics of Zeeman and dipolar states in the spin locking in a liquid entrapped in nanocavities: Application to study of biological systems

Gregory Furman[1,*], **Andrey Kozyrev**[2], **Victor Meerovich**[1], **Vladimir Sokolovsky**[1], **Yang Xia**[3]

[1]Physics Department, Ben Gurion University of the Negev, Beer Sheva, 84105 Israel

[2]Saint-Petersburg Electrotechnical University LETI, Saint-Petersburg, Russia

[3]Physics Department, Oakland University, Rochester, MI, USA

Abstract

We analyze the application of the spin locking method to study the spin dynamics and spin-lattice relaxation of nuclear spins-1/2 in liquids or gases enclosed in a nano-cavity. Two cases are considered: when the amplitude of the radio-frequency field is much greater than the local field acting the nucleus and when the amplitude of the radio-frequency field is comparable or even less than the local field. In these cases, temperatures of two spin reservoirs, the Zeeman and dipole ones, change in different ways: in the first case, temperatures of the Zeeman and dipolar reservoirs reach the common value relatively quickly, and then turn to the lattice temperature; in the second case, at the beginning of the process, these temperatures are equal, and then turn to the lattice temperature with different relaxation times. Good agreement between the obtained theoretical results and the experimental data is achieved by fitting the parameters of the distribution of the orientation of nano-cavities. The parameters of this distribution can be used to characterize the fine structure of biological samples, potentially enabling the detection of degradative changes in connective tissues.

Graphical Abstract

The spin locking method is applied to study the spin dynamics and spin-lattice relaxation of nuclear spins-1/2 in liquids or gases enclosed in a nano-cavity containing water molecules. Here φ is the angel between the main axis Z_c of the cavity and external magnetic field H_0, θ is the angle between the Z_0 -axis given by an averaged orientation of the nano-cavity main axes and the magnetic field, ζ and ξ are the polar and azimuthal angles characterizing the deviation of the main axis Z_c of a cavity from the Z_0 -axis.

We show that measurements of the relaxation parameters and spin temperatures of the Zeeman and dipolar thermodynamic reservoirs provide important information on the size of the cavity, its shape and orientation relative to the magnetic field, and the number of spins in the cavity.

[*]Corresponding author: Phone: +97286472458, FAX: +97286472903, gregoryf@bgu.ac.il (G. B. Furman).

Good agreement between the obtained theoretical results and the experimental data is achieved by fitting the parameters of the distribution of the orientation of nano-cavities. The parameters of this distribution can be used to characterize the fine structure of biological samples, potentially enabling the detection of degradative changes in connective tissues.

polar and azimuthal angles characterizing the deviation of the main axis Z_c of a cavity from the Z_0 -axis.

Keywords

nano-cavity; Zeeman and dipolar reservoirs; spin locking; spin-lattice relaxation 76.60.-k;78.67. Rb

Introduction

Nuclear magnetic resonance (NMR) is widely used to study of structure and dynamic properties of (both organic and inorganic) molecules in solutions, liquid crystals and solids [1, 2]. The study of the dynamics of water molecules inside biological objects by NMR provides important information about the microscopic structure of biological objects. [3–5]. To get the information on the peculiarities of molecular dynamics, the proper choice of specific NMR method is important [1]. This choice depends on the sample structure and on the internal molecular dynamics in tested samples and is determined by NMR response of the nuclear system to the action of an external magnetic field $\vec{H}(t) = \vec{H}_0 + \vec{H}_1(t)$ which is the superposition of the external constant magnetic field $\vec{H}_0$ and the radio frequency (RF) field $\vec{H}_1(t)$, $\left|\vec{H}_0\right| > > \left|\vec{H}_1(t)\right|$. For example, investigation of the spin-lattice relaxation in the laboratory frame by measuring so-called a longitudinal relaxation time T_1 in a large external magnetic field provides information on very fast molecular motion which is characterized by correlation functions with the correlation time $\tau_c \simeq 10^{-12}$ s of the local field.

The fluctuations of the local fields $H_i^{loc}(t)$ acting on the i-th nuclear spin are characterized by the correlation functions $G_{ij}(\tau) = \left\langle H_i^{loc}(t) H_j^{loc}(t+\tau) \right\rangle$ in the conventional theory of NMR relaxation [1]. In many cases including rotational and translational diffusion, the correlation functions can be presented as an exponential function, $G_{ij}(\tau) = \delta_{ij} \overline{H}_{loc}^2 e^{-\frac{\tau}{\tau_c}}$, with a single correlation time τ_c. That leads to the spin-lattice relaxation rates, T_1^{-1} in the laboratory frame [6]:

$$T_1^{-1} = \frac{2}{3} \gamma \overline{H}_{loc}^2 \frac{\tau_c}{1 + \omega_0^2 \tau_c^2}, \quad (1)$$

where $\omega_0 = \gamma \left|\vec{H}_0\right|$ is the Larmour frequency of the nuclei, γ is the gyromagnetic ratio of the nuclei, $\overline{H}_{loc}^2$ is the averaged square of the local magnetic field. For $\omega_0 \tau_c \ll 1, T_1^{-1}$ is independent of ω_0, which is realized e.g. in bulk water with $\tau_c \simeq 10^{-12}$ s. In the opposite

case, $\omega_0\tau_c \gg 1$, the dependence of the relaxation time on the external field is observed and $T_1^{-1} \sim \omega_0^{-2}$, e.g. in ice [7].

Investigation of the spin-lattice relaxation of water in biological tissue has been especially problematic [8]. The study of relaxation time T_1 of water in different tissues is important not only for understanding of the fundamental biophysical chemistry problems but also for many practical problems such as the application technique of NMR imaging to living systems [8, 9]. It was shown in lots of biological tissues there are additional mechanisms of the spin-lattice relaxation with correlation times much longer than 10^{-12}s [10]. To explain the long correlation times in biological samples several models considering various mechanisms of spin-lattice relaxation were proposed [11–14]. These mechanisms are associated with relaxation of the solid-like proton in protein, the anisotropic rotation of adsorbed molecules, and the slow translational diffusion in the hydration layer. Recently, the model based on averaging the Brownian motion of water molecules inside nano-cavities and fluctuations of the cavity walls was developed to explain a long correlation time [15]. Biological tissues such as tendon, articular cartilage, nasal cartilage, cornea and sclera of the eye [8] can be considered as consisting of a set of nano-cavities containing water. It was shown experimentally and theoretically that the relaxation times in nano-cavities significantly differ from these times for bulk water and they depend on the sample orientation relative to the external magnetic field $\vec{H}_0$ [8, 15–21].

Study of the spin-lattice relaxation in the rotating frame, in so-called spin-locking state, gives important information about slow motion of atoms and molecules, which cannot be obtained from measurement of relaxation in strong external fields $\vec{H}_0$.

In the rotating frame the relaxation time $T_{1\rho}$ is more sensitive to slow fluctuations which are characterized by typical correlation times from a few 10^{-5}s to 10^{-3}s [6]. The spin-locking scheme of an excitation is usually implemented by applying the phase shifted two-pulse sequence [22]. This method consists in bringing the magnetization to be parallel to an effective field in the rotating frame by applying a 90° short pulse followed by a 90° phase shift long RF pulse [22]. Application the spin locking method for study of the spin-lattice relaxation in water confined in nano-objects such as nano-pores and nano-cavities promises great advantages and provides information on motion-restricted environment for water molecules [8, 20].

Furthermore, nano-objects possesses unique physical and chemical properties that differ from properties of bulk materials of the same chemical content and structure [23]. One of these unique phenomena is manifested by the fact that intermolecular dipole-dipole interactions (DDI) between nuclear spins in gases or liquids entrapped in nano-cavities are not averaged to zero [24], as usually happens for bulk magnetically isotropic gases or liquids [25]. The averaged dipolar coupling constant depends on the volume and shape of the nano-cavity and its orientation relatively to the external magnetic field [24, 26–28]. As a result, this effect may be used to obtain from the NMR experiment results useful information on the structure of samples containing nanosized objects [15–21, 29]

In this paper we analyze application of the spin-locking technique to the investigation of the spin dynamics and spin-lattice relaxation for the spins-1/2 nuclei in a liquid entrapped in nano-cavities. We show that measurements of the relaxation parameters and spin temperatures of the Zeeman and dipolar thermodynamic reservoirs provide important information on the size of the cavity, its shape and orientation relative to the magnetic field, and the number of spins in the cavity.

Spin locking state in a liquid in nano-cavities

Let us consider a water containing N spins-1/2 nuclei, confined in an elongated nano-cavity in the strong external magnetic field $\vec{H}_0$ (Fig. 1). Molecular motion results in an averaged spin-spin interaction which can be evaluated from the average over orientation and position for many spins. Therefore, the spin dynamics is described by the averaged spin Hamiltonian [15–21]

$$H = H_z + \overline{H}_d + H_{RF}(t), \tag{2}$$

where H_Z is the Zeeman Hamiltonian

$$H_z = \omega_0 I_z, \tag{3}$$

$\overline{H}_d$ is the averaged DDI Hamiltonian [26, 27]

$$\overline{H}_d = G \sum_{i<j} \left(3 I_{zi} I_{zj} - \vec{I}_i \vec{I}_j \right) \tag{4}$$

where $H_{RF}(t)$ is the Hamiltonian of the interaction of nuclear spins with RF field, I_{zj} is the projections of the spin operator $\vec{I}_j$ onto the z- axis of the j-th nuclear spin, G is the space-independent pair-averaged coupling constant which is the same for any pair of spins i and j [26, 27] and for a single axisymmetric cavity is

$$G = -\frac{\gamma^2 \hbar}{V} P_2(\cos\varphi) F, \tag{5}$$

V is the cavity volume and F is the form-factor characterizing the nano-cavity form and varies from $-4\pi/3$ to $2\pi/3$ for ellipsoidal cavities, and $F = 2\pi/\sqrt{1+(2d/l)^2}$ for cylindrical ones, d and l are the diameter and length of the cavity, respectively, φ denotes the angle between main axis of the cavity and the external magnetic field $\vec{H}_0$ and determined by the angles ξ, ζ, and θ in Fig. 1; where θ denotes the angle between the averaged axis of the main cavity axes and the external magnetic field. Expressions (4) and (5) are valid if the characteristic cavity size is less 700 nm [18,19,20]. The averaged DDI Hamiltonian (4) can be rewritten in the following form [27]

$$\overline{H}_d = \frac{G}{2} \left(3 I_z^2 - \vec{I}^2 \right), \tag{6}$$

where $\vec{I}^2 = I_x^2 + I_y^2 + I_z^2$ is the square of the total nuclear spin operator and $I_\mu = \sum_i I_{\mu i}$ is the i operator of the projection of the total spin operator onto the μ-axis ($\mu = x, y, z$).

The Hamiltonian $H_{RF}(t)$ describes the action of RF field on the spin system after the first $\left(\frac{\pi}{2}\right)_y$ - pulse along the y-axis [22]

$$H_{RF}(t) = 2\omega_1 I_x \cos\omega_{RF} t, \tag{7}$$

where $\omega_1 = \gamma\left|\vec{H}_1\right|, \omega_{RF}$ is the frequency of the RF field. Application of a 90° phase shift long RF pulse along the x- axis makes the magnetization locked parallel to this direction in the rotating frame. At the exact resonance frequency of the spins, $\omega_{RF} = \omega_0$, the effective Hamiltonian in the rotating frame is

$$H_{eff} = \omega_1 I_x + \overline{H}_d . \tag{8}$$

The averaged DDI Hamiltonian $\overline{H}_d$ (6) can be divided into a secular part with respect to I_x

$$H_s = -\frac{G}{4}\left(3I_x^2 - \vec{I}^2\right), \tag{9}$$

and a non-secular part

$$H_{ns} = \overline{H}_d - H_s = -\frac{3G}{8}\sum_{m=-2}^{2} T_{2,m} \tag{10}$$

where $T_{2,m} = \sum_{j \neq i} T_{2,m}^{ij}$ are the second rank tensor operators [30, 31].

The spin system can be characterized by the two integrals of motion $\omega_1 I_x$ and H_s. The considered system should reach a quasi-equilibrium state in a spin-spin relaxation time $T_2 \sim \frac{1}{\omega_{loc}}$, where ω_{loc} is the local dipolar field [32]

$$\omega_{loc} = \sqrt{\frac{Tr\left(\overline{H}_d^2\right)}{TrI_z^2}} = \left|\frac{G}{2}\sqrt{3N}\right| = \gamma^2\hbar\left|P_2(\cos\theta)\right|F\sqrt{\frac{3C}{V}}, \tag{11}$$

where $C|$ is a concentration of the nuclear spins. The quasi-equilibrium state is characterized by two different inverse temperatures, and the density matrix of the spin system is:

$$\rho_{eq} = 1 - \alpha\omega_1 I_x - \beta\overline{H}_s, \tag{12}$$

where α and β are the inverse temperatures of the Zeeman and dipolar thermodynamics reservoirs, respectively.

Evolution of spin system in spin locking state

After the establishment of a quasi-equilibrium state, two processes take place in the further evolution of the spin system. The first process is the energy exchange between the Zeeman and the dipolar reservoirs with the mixing rate W. This process is under the effect of the perturbation given by Eq. (10). The operator of the Hamiltonian H_{ns} does not commute either with $\omega_1 I_x$ or with H_s. The second process is the spin-lattice relaxation of the Zeeman and dipolar energies with the relaxation times $T_{1\rho}$ and $T_{1\rho}$. The equations describing the time evolution of the inverse temperatures α and β can be derived using a well-known procedure [22, 33] and it is entirely analogous to the derivation of the Provotorov equations [34]. To include the effect of environment fluctuations, the spin-lattice relaxation, spin-lattice relaxation terms should be added, as it was done earlier [22, 35]. The evolution equations take the following form [36]

$$\begin{aligned} \frac{d\alpha}{dt} &= -W(\alpha-\beta) - T_{1\rho}^{-1}(\alpha-\alpha_L), \\ \frac{d\beta}{dt} &= W\frac{\omega_1^2}{\omega_{loc}^2}(\alpha-\beta) - T_{1d}^{-1}(\beta-\beta_L), \end{aligned} \tag{13}$$

where $\beta_L = \frac{1}{k_B T_L}$, $\alpha_L = \frac{\omega_0}{\omega_1}\beta_L$, T_L is the lattice temperature and k_B is the Boltzmann constant.

The first terms of the right-hand side equations (13) describe the evolution of the inverse temperatures α and β towards to their common value with the mixing rate [36]

$$W = \omega_{loc}\sqrt{\frac{3\pi}{2}}\exp\left[-\frac{2}{3}\left(\frac{\omega_1}{\omega_{loc}}\right)^2\right] \tag{14}$$

and the second terms - achieving equilibrium state of the spin system and the lattice due to the spin-lattice relaxation process [36–38]. The rate $T_{1\rho}^{-1}$ of the Zeeman energy due to the spin-lattice relaxation is [36]

$$T_{1\rho}^{-1} = \frac{6}{5}\frac{\omega_{loc}^2\tau_c}{1+(2\omega_1\tau_c)^2} \tag{15}$$

and the rate T_{1d}^{-1} of the dipolar energy due to this relaxation is

$$T_{1d}^{-1} = \frac{8}{5}\frac{\omega_{loc}^2\tau_c}{1+(2\omega_1\tau_c)^2}. \tag{16}$$

At $\omega_1\tau_c << 1$ both the relaxation times, $T_{1\rho}$ and T_{1d}, are independent of the RF field strength, while at $\omega_1\tau_c \gg 1 T_{1\rho}$ and T_{1d} are proportional to ω_1^2.

The initial conditions can be determined analyzing energy exchange between the Zeeman and dipole reservoirs during the time T_2 after the first short $\left(\frac{\pi}{2}\right)_y$ RF pulse. During the time T_2 the spin systems in both reservoirs are in non-equilibrium states and the energy exchange between them is not described by Eqs. (13). At the RF field strength ω_1 much greater than the local dipolar field $\omega_{loc}(\omega_1 \gg \omega_{loc})$, the exchange process can be neglected during the time T_2 and the initial conditions take the following form

$$\begin{aligned} \alpha(0) &= \frac{\omega_0}{\omega_1}\beta_L, \\ \beta(0) &= \beta_L\,. \end{aligned} \tag{17}$$

In another case, when two quantities ω_1 and ω_{loc} are comparable, a fast exchange occurs between the Zeeman and dipole reservoirs, this leads to equalization of the inverse temperatures α and β during the time of order of T_2. In this case, the initial conditions take the following form

$$\alpha(0) = \beta(0) = \frac{\omega_0}{\omega_1}\beta_L\,. \tag{18}$$

Introducing the following dimensionless variables

$$\begin{aligned} &\bar{\alpha}(\tau) = \frac{\alpha(\tau)}{\beta_L} - 1, \bar{\beta}(\tau) = \frac{\beta(\tau)}{\beta_L} - 1, \tau = Wt, \\ &\bar{\omega} = \frac{\omega_1^2}{\omega_{loc}^2}, q = \left(WT_{1\rho}\right)^{-1}, r = \left(WT_{1d}\right)^{-1} \end{aligned} \tag{19}$$

the evolution equations Eqs. (13) and the initial conditions (17) and (18) can be rewritten in the following forms

$$\begin{aligned} \frac{d\bar{\alpha}}{d\tau} &= -(\bar{\alpha} - \bar{\beta}) - q\bar{\alpha}, \\ \frac{d\bar{\beta}}{d\tau} &= \bar{\omega}(\bar{\alpha} - \bar{\beta}) - r\bar{\beta}, \end{aligned} \tag{20}$$

$$\bar{\alpha}(0) = \frac{\omega_0}{\omega_1}, \bar{\beta}(0) = 0, \tag{21}$$

$$\bar{\alpha}(0) = \bar{\beta}(0) = \frac{\omega_0}{\omega_1}, \tag{22}$$

respectively.

Eqs. (20) have an analytical solution

$$\bar{\alpha}(\tau) = \frac{\bar{\alpha}(0)e^{-\frac{1}{2}\tau Q}}{P}\left[P\cosh\left(\frac{1}{2}\tau P\right) - S\sinh\left(\frac{1}{2}\tau P\right)\right], \tag{23a}$$

$$\bar{\beta}(\tau) = \frac{2\bar{\omega}^2\bar{\alpha}(0)}{P}e^{-\frac{1}{2}\tau Q}\sinh\left(\frac{1}{2}\tau P\right), \tag{23b}$$

with initial conditions (21) and

$$\bar{\alpha}(\tau) = \frac{\bar{\alpha}(0)}{P}e^{-\frac{1}{2}\tau Q}\left[(S-2)\cosh\left(\frac{1}{2}\tau P\right) - P\sinh\left(\frac{1}{2}\tau P\right)\right], \tag{24a}$$

$$\bar{\beta}(\tau) = \frac{\bar{\alpha}(0)}{P}e^{-\frac{1}{2}\tau Q}\left[P\cosh\left(\frac{1}{2}\tau P\right) + (S+2\bar{\omega})\sinh\left(\frac{1}{2}\tau P\right)\right], \tag{24b}$$

with initial conditions (22), respectively.

In Eqs. (23) and (24) we use the notation

$$P = \sqrt{(1+q+r+\bar{\omega})^2 - 4(q+qr+r\bar{\omega})};\ Q = 1+q+r+\bar{\omega};\\ S = 1-q+r-\bar{\omega}\,. \tag{25}$$

We note that coefficients of Eqs. (13) depend on the angle between the cavity's main axis and the external field $\vec{H}_0$ direction and hence both inverse temperatures, of the Zeeman, $\bar{\alpha}(\tau,\theta)$ and dipole $\bar{\beta}(\tau,\theta)$ reservoirs, also depend on the angle. The solutions for the case of $\omega_1 \gg \omega_{loc}$ are presented in Fig. 2. At the magic angle, $\theta = 54.736°$, in the frame of the considered model the energy exchanges between the spin system and the lattice and between the Zeeman and dipole reservoirs are absent and the reservoirs' temperatures are constants. One can see from solutions (24a) and (24b) that inverse temperatures of both the Zeeman $\bar{\alpha}(\tau,\theta)$ and the dipole $\bar{\beta}(\tau,\theta)$ reservoirs are described by two-time exponential dependence with characteristic times $2/(Q+P)$ and $2/(Q-P)$.

One can see from Figs. 2a and 3 that the inverse Zeeman spin temperature $\bar{\alpha}(\tau,\theta)$ decreases monotonically for all orientations of the cavities relative to the magnetic field, with the exception of the orientation angles close to the magic angle, θ = 54.736°. The inverse dipolar spin temperature $\bar{\beta}(\tau,\theta)$ first increases from zero, reaches its maximum value, and then monotonically decreases (Figs. 2b and 3). It should be noted that the maximum of $\bar{\beta}(\tau,\theta)$ depends on the orientation of the cavity relative to the magnetic field.

Fig. 3 illustrates reaching to the common temperature of the Zeeman and dipolar reservoirs at $\omega_1 \gg \omega_{loc}$, i.e. $\bar{\omega} \gg 1,\ \theta = 0.8$ and $\theta = 0.82$. The time of establishing the common temperature and relaxation time required to achieve equilibrium of the spin system with the lattice are strongly dependent on the orientation of the cavity relative to the magnetic field (Fig. 3). In particular, at angle $\theta = 0.8$ the common temperature is reached with the

relaxation time $T_{com} \approx 9$ ms, while at small change of this angle, at $\theta = 0.82$ this time is about 700 ms. The spin-lattice relaxation times $T_{1\rho}$ also differ significantly for these angles: 170 ms and 1050 ms, respectively. The latter relaxation times are determined after establishment of the common temperature of the Zeeman and dipole reservoirs.

At $\omega_1 \leq \omega_{loc}$ i.e. $\bar{\omega} \leq 1$, a fast exchange occurs between the Zeeman and dipole reservoirs, this leads to equalization of the inverse temperatures α and β during the time T_2. After establishing the quasi-equilibrium (12), the both, inverse Zeeman α and dipolar β spin temperatures are described by the solutions (24) with the characteristic times much larger than T_2.

Fig. 4a presents the inverse Zeeman spin temperature $\bar{\alpha}(\tau, \theta)$ as functions of the time and angle which are given by the solutions (24a) with the initial conditions (22). Note that in this case, the inverse spin temperature of the dipole reservoir is some different from that of the Zeeman reservoir (Fig. 4b).

We obtain that variations of the temperatures are different for $\omega_1 \gg \omega_{loc}$ and $\omega_1 \leq \omega_{loc}$: in the first case the common temperature establishes relatively fast and then it slowly approaching the lattice temperature. In the second case the reservoirs' temperatures are approaching separately to the lattice temperature.

Spin-lattice relaxation of the Zeeman and dipolar inverse temperatures under spin locking in tendon.

The theoretical approach developed above can be used for description of the experimental data obtained for a set of perfectly ordered nano-cavities, when all nano-cavities are oriented in the same direction relative to the external magnetic field.

In real samples a deviation from the perfectly-ordered nano-cavities is usually observed. To compare with experimental data, let us consider a system of nanocavities with the orientations distributed over angles ζ and ξ (Fig. 1). We assume that an averaged direction of the Z_c - axes of the nano-cavities is along the Z_0 -axis which creates the angle θ with the external magnetic field. For each nano-cavity the time dependences of temperatures are determined by the cavity orientation relative to the magnetic field. In the NMR experiment the measured value is an angleaveraged one. Here we assume that the distributions over the polar ζ and azimuthal ξ angles are given by the Gaussian ones. The Gaussian distribution functions well simulate the cavity orientations in biological samples [39]. The averaged inverse temperatures can be determined as:

$$\frac{\langle \eta_k(\theta,\tau)\rangle_{\zeta,\xi}}{\langle \eta_k(\theta,0)\rangle_{\zeta,\xi}} = \frac{1}{\langle \eta_k(\theta,0)\rangle_{\zeta,\xi}} \int_0^{2\pi} d\xi \int_0^{\pi} d\zeta \sin(\zeta) \Psi(\zeta,\xi) \eta_k(\theta,\zeta,\xi,\tau), \; k = 1,2 \tag{26}$$

where $\eta_1(\theta,\zeta,\xi,\tau) = \bar{\alpha}(\theta,\zeta,\xi,\tau)$, $\eta_2(\theta,\zeta,\xi,\tau) = \bar{\beta}(\theta,\zeta,\xi,\tau)$ and $\Psi(\zeta,\xi)$ is the distribution function

$$\Psi(\zeta,\xi) = \exp\left[-\left(\frac{\zeta-\zeta_0}{2\sigma_\zeta}\right)^2 - \left(\frac{\xi-\xi_0}{2\sigma_\xi}\right)^2\right] \tag{27}$$

Comparing the experimental and theoretical results, we determine the fitting parameters $\sigma_\zeta, \sigma_\xi, \zeta_0$, and ξ_0. These parameters can be used to characterize the sample structure [17–21].

Substituting expressions (23) or (24) into (26) and integrating we obtain the normalized averaged inverse Zeeman temperature which is proportional to the NMR signal and to the normalized averaged inverse dipolar temperature corresponding to the dipolar signal measuring in phase with the RF field.

We compare our theoretical results with the experimental data for the NMR signal presented in literature [40]. The NMR signal is calculated using Eq. (26) at $\theta = 55°$ and taking the concentration of the nuclear spins of $C = 66\frac{spin}{nm^3}$, the cavity volume V=2000 nm, the form-factor for a long cylindrical cavity $F = 2\pi$, and the correlation time $\tau_c = 3 \cdot 10^5 s$. The NMR signal is proportional the inverse Zeeman temperature and is described by two-exponential temporal function.

The best matching of the calculation results for all four data sets (ω_1 = 500Hz, 1000Hz, 3000Hz, 5000Hz) is achieved at the standard deviations of $\sigma_\zeta = \sigma_\xi = 0.1$ and $\zeta_0 = 2$, $\xi_0 = 0$ (Fig. 5). One can see a more slowly decay of the signal with an increase in the spin-locking field, ω_1.

The polar ζ_0 and azimuthal ξ_0 angles describe the average deviation of the main axes of the nano-cavities from the sample axis. While the standard deviations σ_ζ and σ_ξ describe the spread of the main axes of the nano-cavities from the average direction. The standard deviations σ_ζ and σ_ξ can be used as criterions of the normal anatomical structure and variation of the parameters can indicate a disease or pathological process.

Note, that the local dipolar field depends on the size and shape of the nano-cavities and any variation of the nano-cavity characteristics causes changes in the MRI signal.

Fig. 6 illustrates the time dependence of the inverse Zeeman and dipolar temperatures that are averaged using (26) in the case of high strength field of spin-locking ($\omega_1 \gg \omega_{loc}$) at $\theta = 55°$ and ω_1 = 3000 Hz. The averaged inverse dipolar temperature first increases very sharply and equalizes with the inverse Zeeman temperature, and then both temperatures are achieved the inverse lattice temperature, β_L.

Conclusion

This paper show that it is possible to extract important information about the nano-cavity sample structure as well as about nano-cavities, such as their volume, shape and concentration of nuclear spins, from NMR and high-resolution MRI experiments measuring relaxation times under spin locking conditions. Using the obtained exact solutions of the equations describing the spin dynamics in a liquid enclosed in a nano-cavity, we show that the dipolar interactions play an essential role in the evaluation of the spin systems. Consideration of the dipolar interactions allows us to explain the two-time exponential

dependence of NMR signal, dependences on a sample orientation relative to the external magnetic field, on the nano-cavity orientation distribution as well as on the strength of the spin-locking field. In particular, the initial conditions for equations describing the temperatures' evolutions are determined by the relationship between the spinlocking field strength ω_1 and the local dipolar field ω_{loc}.

When $\omega_1 \gg \omega_{loc}$ the initial conditions are given by (17): the initial inverse temperature of the Zeeman reservoir is $\alpha(0) = \frac{\omega_0}{\omega_1}\beta_L$ and the dipolar one is $\beta(0) = \beta_L$. When $\omega_1 \leq \omega_{loc}$, the initial conditions are $\alpha(0) = \beta(0) = \frac{\omega_0}{\omega_1}\beta_L$. In these two cases the temperatures vary differently: in the first case temperatures of the Zeeman and dipolar reservoirs relatively fast reach a common one and then approaching the lattice temperature; in the second case the temperatures initially are equal and then are separately approached the lattice one.

We have obtained good agreement between the theoretical results and the experimental data by using the nano-cavity orientation distribution as the adjustment parameter. The fitting parameters of this distribution can be used to characterize the fine structures of fiber-like biological samples. Good agreement between the theoretical and experimental results was achieved at the standard deviation, $\sigma_\zeta = \sigma_\xi = 0.1$, which allows one to suggest that the tendon mainly composed of collagen and water molecules is a highly ordered structure. The developed approach in our model opens a sensitive and non-invasive way to determine local changes in the microstructure of tissues using the microscopic MRI data, for example changes in fibril structures in tendons and ligaments due to autoimmune diseases such as rheumatoid arthritis and sarcoidosis.

Acknowledgement

This research was supported by a grant from the United States - Israel Binational Science Foundation (BSF), Jerusalem, Israel (2019033), and by a grant from the National Institutes of Health in the United States (AR 069047).

References

1. Abragam A, The Principles of Nuclear Magnetism, Oxford Clarendon Press, 1961.
2. de Gennes PG and Prost J, The Physics of Liquid Crystals, Oxford Clarendon Press, 1995.
3. Callaghan PT, Principles of Nuclear Magnetic Resonance Microscopy, Oxford Clarendon Press, 1991.
4. Breitmaier E, Structure Elucidation by NMR in Organic Chemistry: A Practical Guide, John Wiley&Sons Ltd., 2002
5. Alba-Simionesco C, Coasne B, Dosseh G, Dudziak G, Gubbins KE, Radhakrishnan R. and Sliwinska-Bartkowiak M, Effects of confinement on freezing and melting, J. Phys.: Condens. Matter 18 R15 (2006).
6. Slichter CP, Principles of Magnetic Resonance, p. 153, Harper & Row, New York, 1963.
7. Glasel J, in Water (Franks F, Ed.), Vol. 1, Chap. 6, pp. 215–254, Plenum, New York.
8. Xia Y. and Momot K, Biophysics and Biochemistry of Cartilage by NMR and MRI, The Royal Society of Chemistry, Cambridge UK, 2016.
9. Koenig SH and Brown RD, A molecular theory of relaxation and magnetization transfer: application to cross-linked BSA, a model for tissue. Magn Reson Med 1993; 30:685–695. [PubMed: 8139450]

10. Halle B, Molecular Theory of Field-Dependent Proton Spin-Lattice Relaxation in Tissue, Magn Reson Med, 56, 60–72 (2006). [PubMed: 16732594]
11. Fung BM, Proton and deuteron relaxation of muscle water over wide ranges of resonance frequencies, Biophys. J 18, 235 (1977). [PubMed: 861361]
12. Held G, Noack F, Pollak V, and Melton B, Naturforch Z. Sect. C. Biosci 28, 59 (1973).
13. Koenig SH, The dynamics of water-protein interactions, in Water in Polymers (Rowland SP, Ed.) ACS Symp. Series No. 127, 157, (1980)
14. Bottomley PA, Foster TH, Argersinger RE, and Pfeifer LM, A review of normal tissue hydrogen NMR relaxation times and relaxation mechanisms from 1–100 MHz: dependence on tissue type, NMR frequency, temperature, species, excision, and age, Med. Phys 11, 425 (1984). [PubMed: 6482839]
15. Furman GB, Goren SD, Meerovich VM, and Sokolovsky VL, Multiple-pulse spinlocking in nanofluids, RSC Adv. 5 (2015) 44247.
16. Furman GB, Goren SD, Meerovich VM, and Sokolovsky VL, Nuclear spin--lattice relaxation in nanofluids with paramagnetic impurities, JMR 261 (2015) 175–180. [PubMed: 26583530]
17. Furman GB, Goren SD, Meerovich VM, and Sokolovsky VL, Anisotropy of spin-spin and spin--lattice relaxation times in liquids entrapped in nanocavities: Application to MRI study of biological systems, JMR 263 (2016) 71–78. [PubMed: 26773529]
18. Furman GB, Goren SD, Meerovich VM, and Sokolovsky VL, Correlation of transverse relaxation time with structure of biological tissue, JMR 270 (2016) 7–11. [PubMed: 27380185]
19. Furman GB, Goren SD, Meerovich VM, and Sokolovsky VL, Dipole-dipole interactions in liquids entrapped in confined space, J. Mol. Liq 272 (2018) 468–473.
20. Furman G, Meerovich V, Sokolovsky V, and Xia Y, Spin locking in liquid entrapped in nanocavities: application to study connective tissues, J. Magn. Reson 299 (2019) 66–73. [PubMed: 30580046]
21. Furman G, Meerovich V, Sokolovsky V, and Xia Y, Spin-lattice relaxation in liquid entrapped in a nanocavity, JMR 311, 106669 (2020).
22. Goldman M, Spin Temperature and Nuclear Resonance in Solids, Oxford Clarendon Press, 1970.
23. Korb JP, Malier L, Cros F, Xu S, and Jonas J, Surface Dynamics of Liquids in Nanopores, Phys. Rev. Let, 77, 2312 (1996). [PubMed: 10061912]
24. Baugh J, Kleinhammes A, Han D, Wang Q, and Wu Y, Confinement Effect on DipoleDipole Interactions in Nanofluids, Science, 294, 1505 (2001). [PubMed: 11711669]
25. Richter W. and Warren WS, Intermolecular multiple quantum coherences in liquids, Concepts Magn. Reson, 12, 396 (2000).
26. Rudavets MG and Fel'dman EB, Nonergodic dynamics of a system of nuclear spins 1/2 with identical spin-spin coupling constants, JETP Letters, 75, 635–637 (2002).
27. Fel'dman EB and Rudavets MG, Nonergodic nuclear depolarization in nanocavities, JETP, 98, 207 (2004).
28. Doronin SI, Fedorova AV, Fel'dman EB, and Zenchuk AI, J. Chem. Phys 131, 104109 (2009).
29. Tsukahara T, Mizutani W, Mawatari K, and Kitamori T, NMR Studies of Structure and Dynamics of Liquid Molecules Confined in Extended Nanospaces, J. Phys. Chem. B 113, 10808 (2009). [PubMed: 19603763]
30. Edmonds R, Angular Momentum in Quantum Mechanics, Princeton, New Jersey: Princeton University Press (1957).
31. Haeberlen U, High Resolution NMR in Solids, Academic Press, 1978.
32. Doronin SI, Fel'dman EB, and Zenchuk AI, The multiple quantum NMR dynamics in systems of equivalent spins with a dipolar ordered initial state, J. Exp. Theor. Phys, 113, 495 (2011).
33. Zubarev DN, Nonequilibrium Statistical Thermodynamics, Imprint Consultants Bureau, New York, 1974.
34. Provotorov BN, Magnetic Resonance Saturation in Crystals, Soviet Physics --- JETP 14, 1126 (1962).
35. Fel'dman EB and Rudavets MG, NMR line shapes of a gas of nuclear spin-12 molecules in fluctuating nano-containers, Chemical Physics Letters 396, 458 (2004).

36. Fel'dman EB, Furman GB, and Goren SD, Spin locking and spin--lattice relaxation in a liquid entrapped in nanosized cavities, Soft Matter, 8, 9200 (2012)

37. Haberlen U. and Waugh JS, Phys. Rev, 185, 420 (1969).

38. Mehring M, High Resolution NMR Spectroscopy in Solids, Springer-Verlag, 1978.

39. Navon G, Eliav U, Demco DE, and Blümich B, Study of order and dynamic processes in tendon by NMR and MRI, J Magn Reson Imaging, 25, 362–380 (2007). [PubMed: 17260401]

40. Wang N. and Xia Y, Anisotropic Analysis of Multi-component T2 and T1ρ Relaxations in Achilles Tendon by NMR Spectroscopy and Microscopic MRIJ Magn Reson Imaging. 38, 625–633 (2013).

*** Highlights (for review)**

Spin locking method is applied to study the spin dynamics in liquid in a nano-cavity

The kinetic equations describe the spin lattice relaxation in bulk liquid is used.

We explain the two-time exponential dependence of NMR signal

NMR signal dependences on the strength of the spin-locking field are explained.

The good agreement with the experimental data is obtained

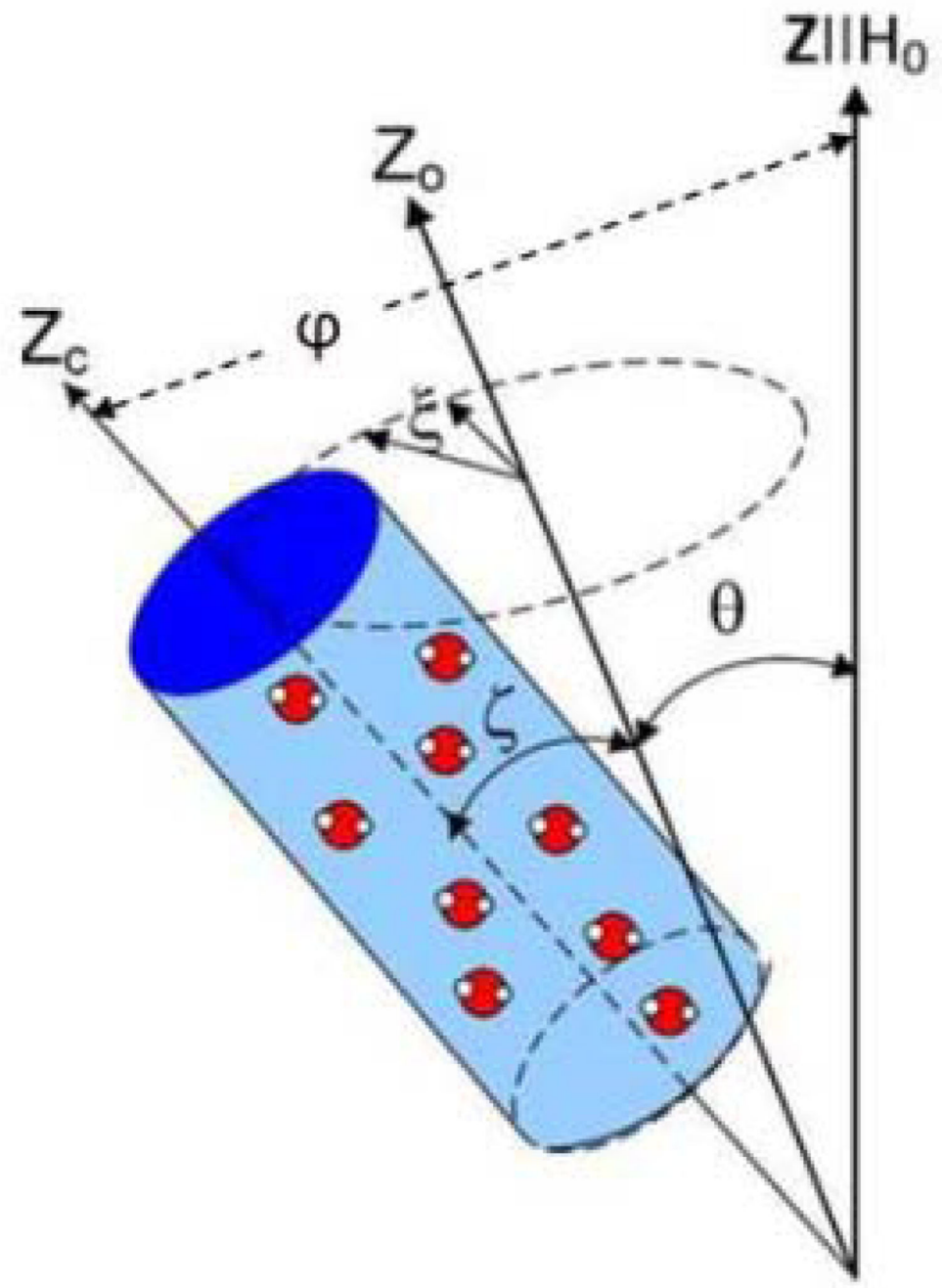

Fig. 1.

A nano-cavity containing water molecules. Here φ is the angel between the main axis Z_c of the cavity and external magnetic field H_0, θ is the angle between the Z_0 -axis given by an averaged orientation of the nano-cavity main axes and the magnetic field, ζ and ξ are the polar and azimuthal angles characterizing the deviation of the main axis Z_c of a cavity from the Z_0 axis.

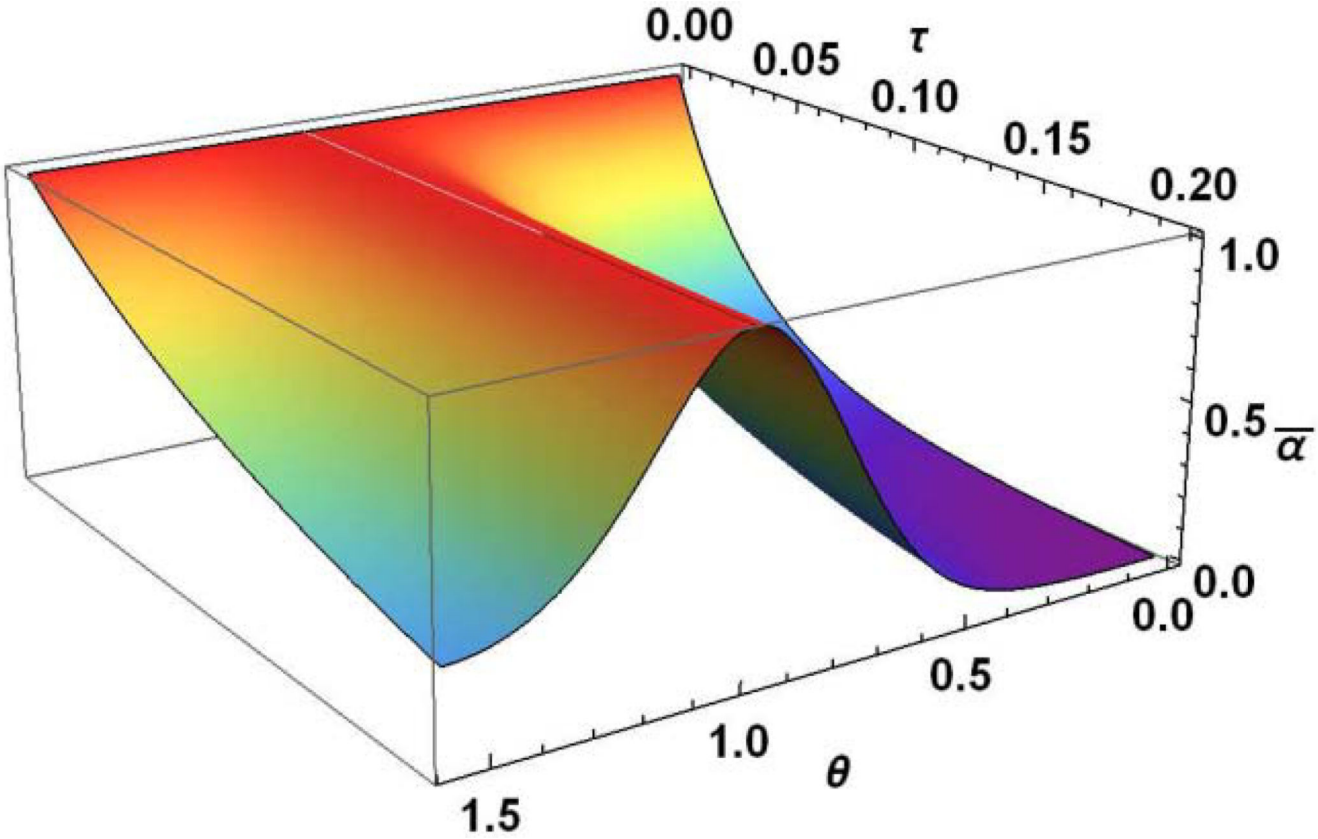

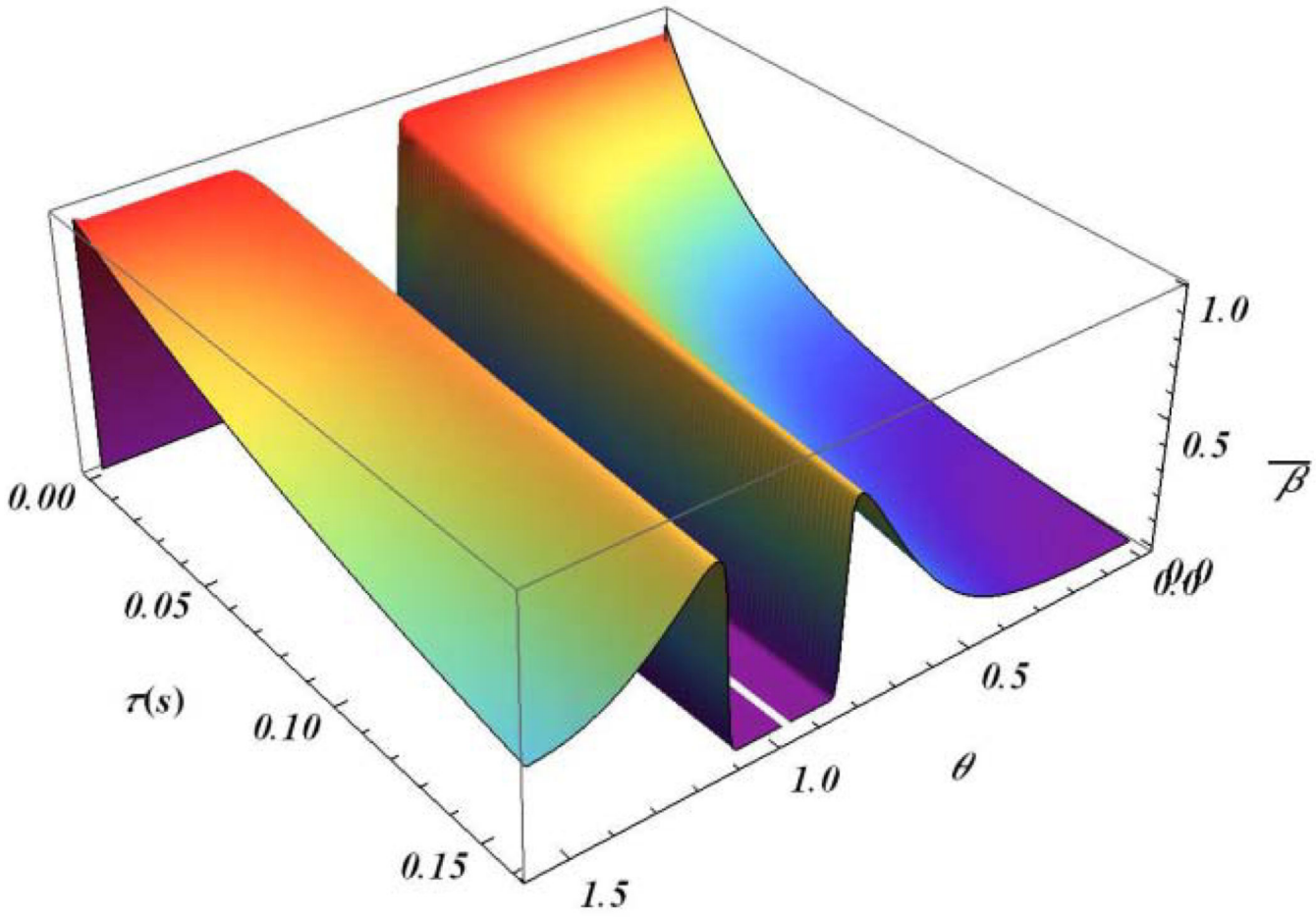

Fig. 2.

Time and angle dependences of the inverse dimensionless spin temperatures of (a) the Zeeman and (b) dipolar reservoirs, calculated using Eqs. (23a) and (23b), respectively.

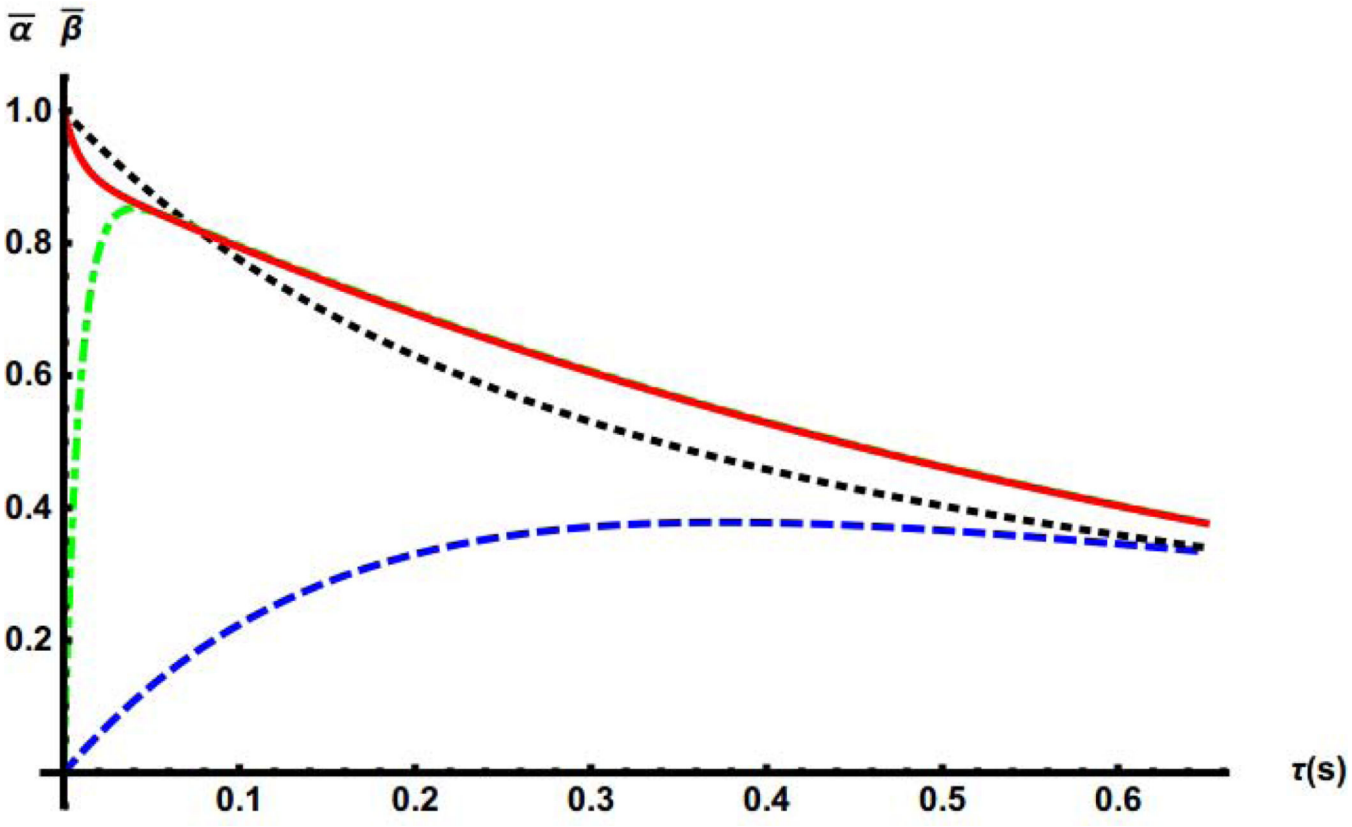

Fig. 3.

Time dependences of the inverse dimensionless spin temperature of the Zeeman reservoir, calculated using Eq. (23a) (red, solid curve - at θ=0.8 rad and black dotted - at θ=0.82 rad) and time dependences of the inverse dimensionless spin temperature of the dipolar reservoir calculated using Eq. (23b) (green, dot-dashed curve - at θ=0.8 rad and blue dashed - at θ=0.82 rad)

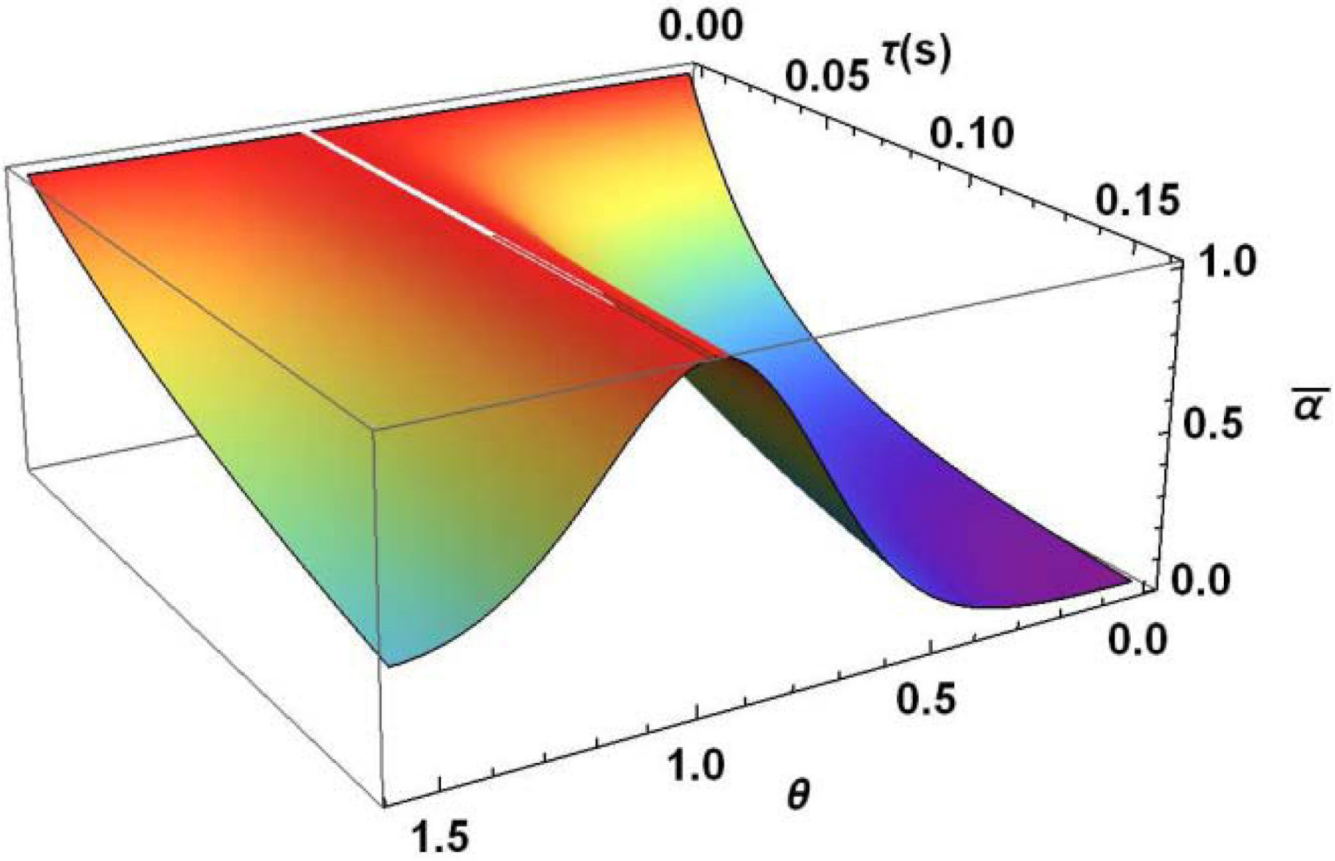

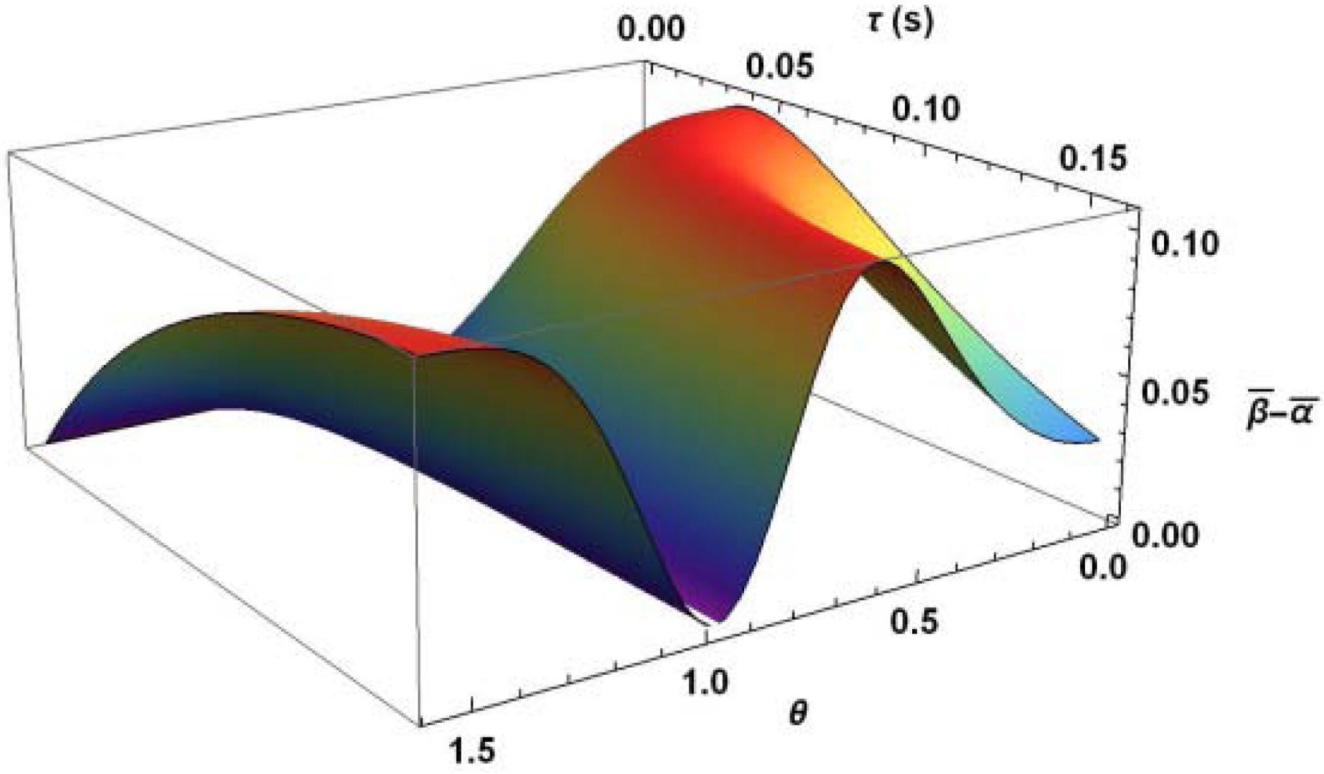

Fig. 4.

(a) Time and angle dependences of the inverse dimensionless spin temperature of the Zeeman reservoir, calculated using Eq. (24a); (b) These dependences of the difference between inverse dimensionless spin temperatures of the Zeeman and the dipolar reservoirs, calculated using Eqs. (24a) and (24b).

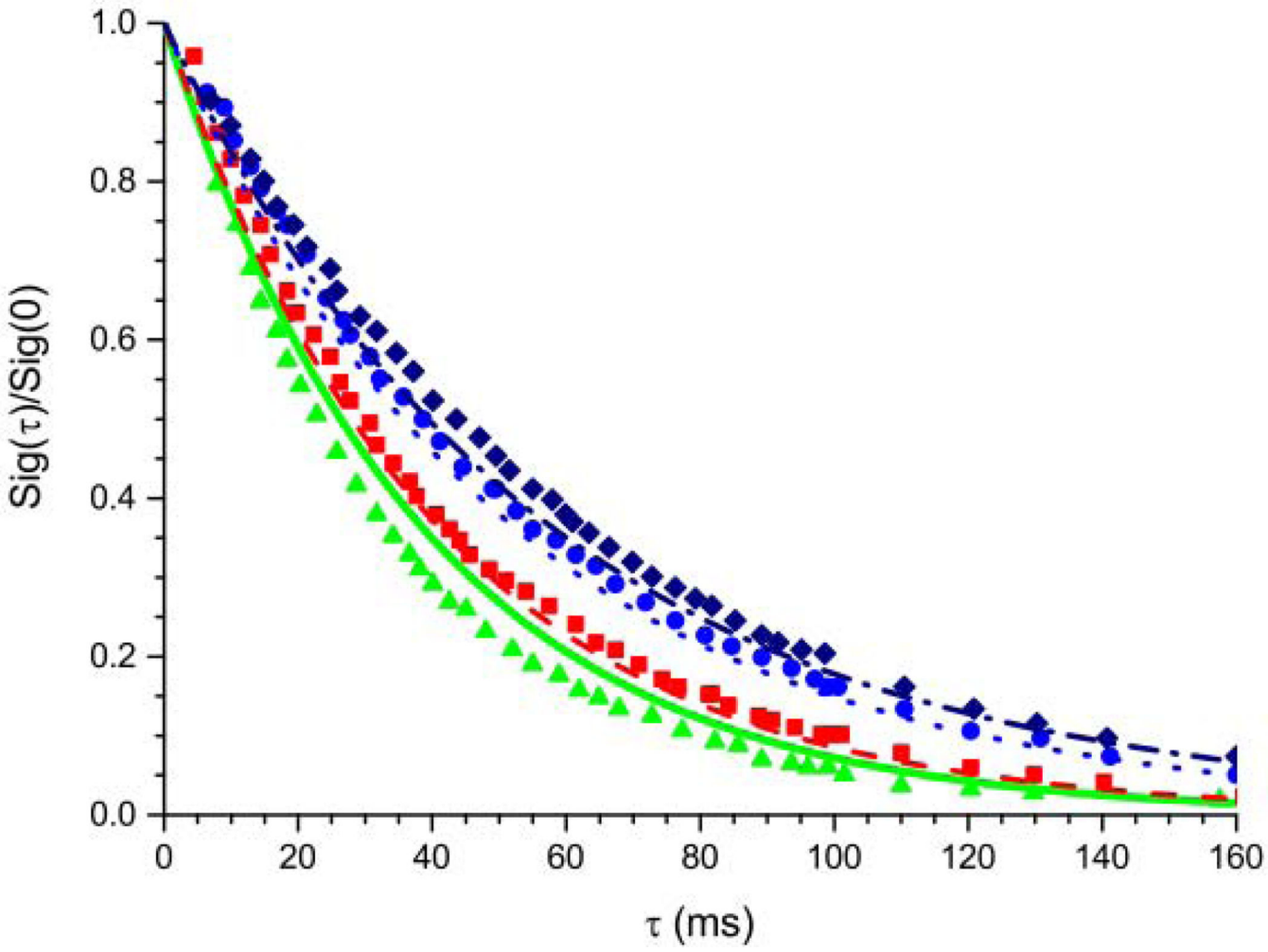

Fig. 5.

The normalized NMR signals of tendon at different strength of spin-locking field is calculated using Eq. (26) and the experimental data from [40]: ω_1 = 500 Hz – green solid curve presents theoretical results and green triangles are the experimental data; ω_1 = 1000 Hz – red dashed curve (theoretical results) and red squares (the experimental data); ω_1 = 3000 Hz – blue dotted curve (theoretical results) and blue circles (the experimental data); ω_1 = 5000 Hz – navy dashed-dotted curve presents theoretical results and navy pentagons are the experimental data. Note that error bars for the experimental date are slowly higher than the symbol sizes.

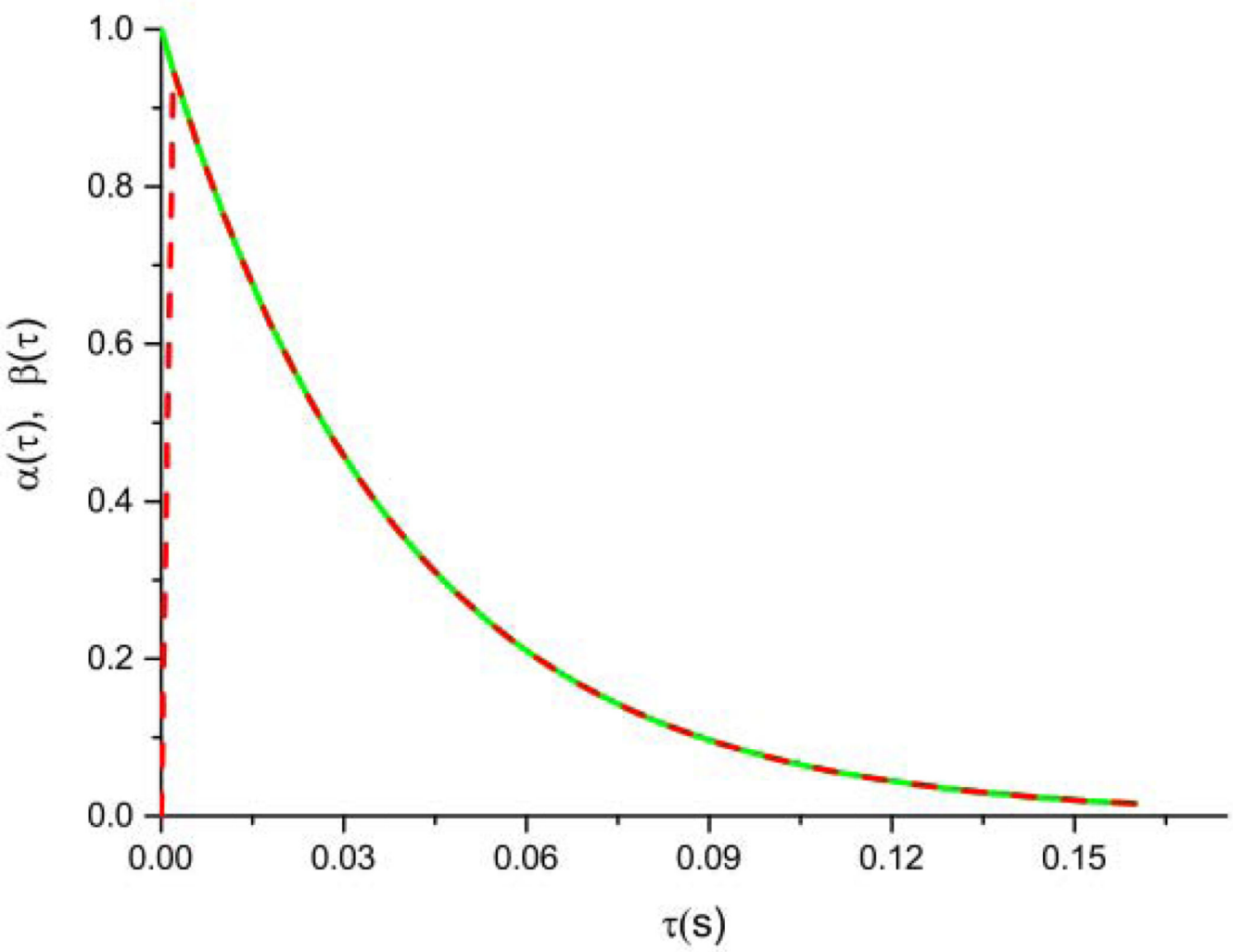

Fig. 6.

Time dependences of the Zeeman and dipolar inverse temperatures in the case of high strength of the spin-locking field ($\omega_1 \gg \omega_{loc}$).